

## RESEARCH ARTICLE

10.1002/2017MS001074

## On the Utility (or Futility) of Using Stable Water Isotopes to Constrain the Bulk Properties of Tropical Convection

Suqin Q. Duan<sup>1</sup> , Jonathon S. Wright<sup>1</sup> , and David M. Romps<sup>2,3</sup> <sup>1</sup>Department of Earth System Science, Tsinghua University, Beijing, China, <sup>2</sup>Department of Earth and Planetary Science, University of California, Berkeley, CA, USA, <sup>3</sup>Climate & Ecosystem Sciences Division, Lawrence Berkeley National Laboratory, Berkeley, CA, USA

## Key Points:

- An analytical model is derived for profiles of H<sub>2</sub>O and HDO in radiative-convective equilibrium
- Mean HDO is insensitive to entrainment and precipitation efficiency at fixed relative humidity
- Mean HDO is not a useful source of information on bulk convective processes below the TTL

## Correspondence to:

S. Duan,  
dsq13@mails.tsinghua.edu.cn

## Citation:

Duan, S. Q., Wright, J. S., & Romps, D. M. (2018). On the utility (or futility) of using stable water isotopes to constrain the bulk properties of tropical convection. *Journal of Advances in Modeling Earth Systems*, 10, 516–529. <https://doi.org/10.1002/2017MS001074>

Received 2 JUN 2017

Accepted 2 FEB 2018

Accepted article online 7 FEB 2018

Published online 23 FEB 2018

**Abstract** Atmospheric water-vapor isotopes have been proposed as a potentially powerful constraint on convection, which plays a critical role in Earth's present and future climate. It is shown here, however, that the mean tropical profile of HDO in the free troposphere does not usefully constrain the mean convective entrainment rate or precipitation efficiency. This is demonstrated using a single-column analytical model of atmospheric water isotopes. The model has three parameters: the entrainment rate, the precipitation efficiency, and the distance that evaporating condensates fall. At a given relative humidity, the possible range of HDO is small: its range is comparable to both the measurement uncertainty in the mean tropical profile and the structural uncertainty of a single-column model. Therefore, the mean tropical HDO profile is unlikely to add information about convective processes in a bulk-plume framework that cannot already be learned from relative humidity alone.

**Plain Language Summary** Several of the the physical processes related to rain clouds are still quite uncertain, and that uncertainty is the largest impediment to developing more accurate forecasts of future climate. It has been proposed that measurements of the heavy water isotope HDO could be a useful means of probing those cloud processes. Here, a simple model is developed for testing the sensitivity of HDO to different cloud processes. The results from this model reveal that HDO is largely insensitive to changes in these parameters at a fixed relative humidity. Unfortunately, then, the average amount of HDO in the atmosphere does not provide any significant constraint on cloud processes that is not already provided by the relative humidity alone.

## 1. Introduction

Stable isotopes in water vapor and precipitation have yielded many important insights. The prevalence of oxygen-18 (H<sub>2</sub><sup>18</sup>O) and deuterium (HDO) in precipitation, as recorded in ice cores, documents past temperatures (Jouzel et al., 1987; Petit et al., 1999; Steffensen et al., 2008; Thompson et al., 1989). H<sub>2</sub><sup>18</sup>O and HDO in cave deposits record past rain rates (Frappier et al., 2007; Higgins & MacFadden, 2004; Lee et al., 2009a). With regards to the current climate, studies of these isotopes have distinguished between bottom-heavy and top-heavy profiles of atmospheric ascent (Torri et al., 2017), differentiated between evaporation and transpiration in the boundary layer (Moreira et al., 1997; Williams et al., 2004), and reduced the uncertainty as to the sources and sinks of water in the tropical tropopause layer (TTL) (Bolot et al., 2017).

But what, if anything, have these isotopes revealed about the processes operating within free-tropospheric deep convection? By “free troposphere,” we mean the layer of the troposphere bounded by the top of the boundary layer and the bottom of the TTL. By “processes,” we mean physical processes such as entrainment and evaporation of precipitation; we exclude from our definition of processes the *state* of deep convection, such as its depth at some particular location (Torri et al., 2017) or its intensity there (Frappier et al., 2007). By these definitions, it can be argued that past studies of stable water isotopes have not taught us anything about free-tropospheric convective processes that we did not already know, or that we could not have learned by other means.

Past studies of deep convection and isotopes can be broadly described as belonging to one of three categories. First, there are papers showing that some numerical model is broadly consistent with the observed

© 2018. The Authors.

This is an open access article under the terms of the Creative Commons Attribution-NonCommercial-NoDerivs License, which permits use and distribution in any medium, provided the original work is properly cited, the use is non-commercial and no modifications or adaptations are made.

distribution of isotopes (e.g., Risi et al., 2010, 2012a). Those studies can assure us that a model is performing adequately, but do not teach us something fundamentally new about convection in the real free troposphere.

Second, there are papers that perturb some parameters in a global climate model (GCM) and look at the behavior of the isotopes (e.g., Bony et al., 2008; Lee et al., 2009b; Nusbaumer et al., 2017; Risi et al., 2012b; Sherwood & Risi, 2012; Tharammal et al., 2017; Wright et al., 2009). Many of these papers propose that isotopes should be useful in constraining convective processes in the real world, but they all stop short of that goal.

Third, there are papers that investigate fractionation processes in the atmosphere (e.g., Berkelhammer et al., 2012; Brown et al., 2008; Kurita et al., 2011; Risi et al., 2008; Worden et al., 2007). Papers in this third category are motivated not by an intrinsic interest in the detailed transport of isotopes – after all, rare water isotopes have no impact on weather and climate – but, instead, are motivated by the hope that a better understanding of fractionation will allow future observations of isotopes to reveal something new about the world.

Here, we investigate whether the mean tropical profile of HDO can tell us something about the bulk deep-convective entrainment rate, the bulk precipitation efficiency, or the typical vertical displacement between the condensation/deposition and evaporation/sublimation of condensates. Notice that we focus here on a mean tropical profile, and we refer to the *bulk* convective processes, which are important for GCM parameterizations. We also restrict our attention to three convective processes in the main text: entrainment, precipitation efficiency, and the mean vertical displacement (lofting/falling) of the precipitation that eventually evaporates or sublimates. For later analysis, when we refer to convective processes, we are referring to these three parameters. They are three of the most uncertain and sought-after parameters in the study of deep convection (e.g., de Rooy et al., 2013; IPCC, 2013; Langhans et al., 2015; Lu et al., 2013, 2016; Romps, 2010, 2016a; Romps & Kuang, 2009; Tao et al., 2004). In Appendix A, we extend the analysis to include fractionation during the evaporation of condensates, but this does not alter the conclusions.

Having defined our question in this way, we can seek answers within a single-column analytical model of radiative-convective equilibrium (RCE), which is a useful starting point for understanding the tropical atmosphere. In particular, we add HDO to a recent analytical model of RCE (Romps, 2014a). The resulting model is depicted in Figure 1. Condensation  $C$  and associated fractionation occur at each height in the ascending cloud plume. A fraction  $\xi$  of those condensates evaporate into the environment a distance  $\Delta z$  below; the remaining  $1-\xi$  precipitate out entirely. There are also equal amounts of entrainment and detrainment, set by the fractional entrainment rate  $\epsilon$ . Together with a prescribed vertical profile of in-cloud water-vapor mass fraction  $q_c$  (subscript  $c$  for cloud), a prescribed mean fractionation factor  $\alpha$ , and a prescribed boundary-layer  $\delta D$ , the three parameters  $\epsilon$ ,  $\xi$ , and  $\Delta z$  determine the environmental profile of  $\delta D_e$  (subscript  $e$  for environment). With this model, it takes only minutes to explore millions of RCE solutions within the three-dimensional parameter space. A detailed derivation of the model is given in section 2; a reader who is satisfied with the level of detail in Figure 1 may wish to skip directly to the results in section 3.

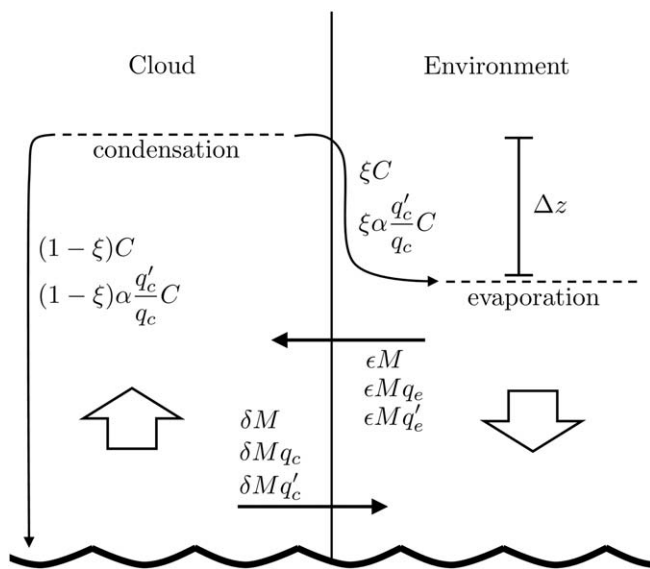


**Figure 1.** Sketch of the analytical model of the tropical atmosphere. In this bulk-plume model, air ascends homogeneously in clouds and descends homogeneously in the environment. Subscripts  $c$  and  $e$  denote cloud and environment, respectively, and  $q$  and  $q'$  denote the mass fractions of H<sub>2</sub>O and HDO, respectively. Mass is exchanged between the cloud and environment through equal rates of entrainment and detrainment (set by the fractional entrainment rate  $\epsilon$ ) and by the evaporation into the environment of a fraction  $\xi$  of the condensates formed within the cloud a distance  $\Delta z$  above. See section 2 for more details.

## 2. The Analytical Model

To build our model of  $\delta D_e$ , we inherit a previous analytical framework for radiative-convective equilibrium (Romps, 2014a) and make an addition to incorporate a heavy water isotope. Convective cloud and the environment are treated as two “bulk plumes,” by which we mean that each of the two plumes has homogeneous properties at each altitude. We use  $q_c$  to denote the mass fraction of H<sub>2</sub>O (i.e., specific humidity) in the cloud plume,  $q_e$  the mass fraction of H<sub>2</sub>O (i.e., specific humidity) in the environment,  $q'_c$  the mass fraction of HDO in cloud, and  $q'_e$  the mass fraction of HDO in the environment. Here, the subscript “ $c$ ” denotes cloud, the subscript “ $e$ ” denotes the environment, and the prime denotes the heavy

isotope. We define  $M$  as the mass flux of the cloud plume (with units of  $\text{kg m}^{-2} \text{s}^{-1}$ ). Because this model is based on RCE, the ascent rate of the environment is  $-M$ , i.e., air in the environment descends at the same rate of mass per area as air in the cloud plume ascends. The model is bounded below by the cloud base. At this lower boundary, air rises up into the cloud plume with mass fractions of  $\text{H}_2\text{O}$  and  $\text{HDO}$  that are set to observed tropical sub-cloud-layer values. For simplicity and analytical solvability, we do not impose an upper boundary on the model. In numerical implementations of this model, the tops of the two plumes are plumbed together such that any mass flux flowing out the top of the cloud plume is fed directly into the top of the environmental plume. In the analytical solutions presented in this paper, however, analytical solvability requires that we do not impose an upper boundary on the model. Equivalently, we can think of the upper boundary as being far above the region of the troposphere we are considering; at a distance of more than a couple kilometers, the influence of the model top is negligible. Note that Figure 1 is not drawn to scale: deep-convective updrafts occupy a small fraction of area in the tropics (on the order of  $10^{-3}$ ), which allows us to approximate the horizontal average of  $\text{H}_2\text{O}$  and  $\text{HDO}$  mass fractions as  $q_e$  and  $q'_e$ , respectively.

As depicted in Figure 1, ordinary water (i.e.,  $\text{H}_2\text{O}$ ) undergoes several processes in this model. In the ascending clouds, water vapor condenses at rate  $C$  (units of  $\text{kg m}^{-3} \text{s}^{-1}$ ). At each height  $z$ , a fraction  $1-\xi$  of the condensates formed at that height are assumed to fall directly to the surface, and the remaining fraction  $\xi$  is assumed to be added to the environment at height  $z-\Delta z$ , where it is assumed to evaporate immediately in the subsaturated environmental air. Note that  $1-\xi$  is the precipitation efficiency and  $\Delta z$  is the distance that evaporating condensates fall between their formation and their evaporation. Another exchange of water between clouds and the environment occurs through turbulent exchange, which is parameterized by the fractional entrainment rate  $\epsilon$  (with units of  $\text{m}^{-1}$ ) and the fractional detrainment rate  $\delta$  (with units of  $\text{m}^{-1}$ ). The rate at which total mass is entrained into the cloud is  $\epsilon M$  (with units of  $\text{kg m}^{-3} \text{s}^{-1}$ ). The rate at which water vapor is entrained into the cloud is  $\epsilon M q_e$ . Similar expressions ( $\delta M$  and  $\delta M q_c$ ) apply to detrainment.

The heavy isotopologue ( $\text{HDO}$ ) is processed in all the same ways, except for the fractionation that occurs upon condensation. Denoting by  $\alpha$  the fractionation factor, the rate at which  $\text{HDO}$  is condensed is  $\alpha(q'_c/q_c)C$ . We assume that the fraction  $\xi$  of those condensates that evaporate do so in entirety, so there is no fractionation that occurs in that step. This is revisited in Appendix A, which finds that the inclusion of this fractionation does not alter the conclusions.

To find steady-state solutions to the system pictured in Figure 1, we must first write down the equations codifying conservation of total mass, light cloud vapor, light environmental vapor, heavy cloud vapor, and heavy environmental vapor:

$$\frac{\partial}{\partial z} M = \epsilon M - \delta M \tag{1}$$

$$\frac{\partial}{\partial z} (M q_c) = \epsilon M q_e - \delta M q_c - C \tag{2}$$

$$\frac{\partial}{\partial z} (-M q_e) = -\epsilon M q_e + \delta M q_c + \xi C (z + \Delta z) \tag{3}$$

$$\frac{\partial}{\partial z} (M q'_c) = \epsilon M q'_e - \delta M q'_c - \alpha \frac{q'_c}{q_c} C \tag{4}$$

$$\frac{\partial}{\partial z} (-M q'_e) = -\epsilon M q'_e + \delta M q'_c + \xi \alpha \frac{q'_c (z + \Delta z)}{q_c (z + \Delta z)} C (z + \Delta z) . \tag{5}$$

These equations depend on three convective parameters whose values in nature are uncertain: the entrainment rate  $\epsilon$ , the precipitation efficiency  $1-\xi$ , and the distance  $\Delta z$  over which condensates descend before they evaporate. The value of  $\delta$  will be set by an assumption on the vertical profile of  $M$ , so it will not be treated as an independent convective parameter.

In previous work (Romps, 2014a), these mass-conservation equations were supplemented with the thermodynamic equation, hydrostatic balance, the ideal-gas law, and the Clausius-Clapeyron relation. The use of those additional equations made it possible to calculate the lapse rate and the RH profile. In the present

study, we simplify matters by using a single exponential profile for  $q_c$  in the free troposphere,  $q_c(z) = q_c(0) \exp(-\gamma z)$ , where  $\gamma$  is a constant,  $z = 0$  is base of the free troposphere, and  $q_c(0)$  is the specific humidity at the base of the free troposphere. This simplified expression for the  $q_c$  profile eliminates the need for all of those additional equations. Most critically, it makes the system of equation analytically solvable, and it produces results that are quantitatively similar to numerical solutions with realistic profiles of  $q_c$ . The constant value used here is  $\gamma = -\partial \log(q_c) / \partial z = 0.5 \text{ km}^{-1}$ , which is chosen to connect  $q_c(0) = 21 \text{ g kg}^{-1}$  (the ERA-Interim tropical mean surface specific humidity, which approximates the cloud-base value in a well-mixed boundary layer) to  $q_c(15 \text{ km}) = 1.3 \times 10^{-2} \text{ g kg}^{-1}$  (the ERA-Interim tropical mean 15-km saturation specific humidity with respect to liquid; for simplicity, all condensates are treated as liquids).

Another simplification is the assumption that the cloud and environment are at the same temperature at each height. In the tropics, the typical virtual temperature difference between a convecting cloud and its environment is only about 0.3–0.5 K (Romps & Öktem, 2015). This observation has led to the zero-buoyancy approximation (Singh & O’Gorman, 2013), which treats the actual temperature difference as zero, and which has been used to successfully derive accurate expressions for tropical CAPE (Romps, 2016b; Seeley & Romps, 2016a, 2016b; Singh & O’Gorman, 2013) and relative humidity (Romps, 2014a). Adopting this approximation,  $q_c$  then equals the environment’s saturation specific humidity, which allows us to write  $q_e = RH q_c$ .

To ensure analytic solvability, we must also set the equilibrium fractionation factor  $\alpha$  to be a constant. In reality,  $\alpha$  is a function of temperature, increasing from 1.1 in the lower troposphere to 1.3 in the upper troposphere. Here, we take a constant value of  $\alpha = 1.17$  throughout the troposphere, which, in the solutions with plausible  $\epsilon$ , plausible  $\xi$ , and  $\Delta z = 2 \text{ km}$ , connects up a surface  $\delta D$  of  $-80\text{‰}$  with a value around  $-700$  to  $-650\text{‰}$  at 15 km. In sensitivity tests, adding  $\pm 0.01$  to our constant choice of  $\alpha$  alters the  $\delta D$  at 15 km by about  $\pm 20\text{‰}$ , but does not alter any of the conclusions about how sensitive the  $\delta D$  profiles are to other parameters. Likewise, prescribing the vertical profile of  $\alpha$  as a function of temperature (to give the observed  $q_c$  profile) would not alter the conclusions either.

The final simplification is to assume constant and equal entrainment and detrainment rates ( $\epsilon = \delta$ ), which gives a constant mass flux  $M$ . This simplification is justified by the similar values of entrainment and detrainment throughout most of the free troposphere (Romps, 2014b). Taking the model top to be infinitely high, the solution to H<sub>2</sub>O equations (2) and (3) is

$$C = [\gamma - \epsilon(1 - RH)] M q_c \tag{6}$$

$$RH = \frac{\epsilon + a \xi \gamma - a \xi \epsilon}{\epsilon + \gamma - a \xi \epsilon} \tag{7}$$

$$q_c(z) = q_c(0) e^{-\gamma z} \tag{8}$$

$$q_e(z) = RH q_c(0) e^{-\gamma z}, \tag{9}$$

where  $a = e^{-\gamma \Delta z}$ .

To solve for the HDO profiles, we can try a solution of the form  $q'_c(z) = q'_c(0) \exp(-\gamma' z)$  and  $q'_e(z) = RH' q'_c(z)$ , where  $\gamma'$  and  $RH'$  are constants. We can think of  $RH'$  as the HDO humidity in the environment relative to the HDO humidity in the cloud, just as  $RH$  is the H<sub>2</sub>O humidity in the environment relative to the H<sub>2</sub>O humidity in the cloud. Using this ansatz of an exponential  $q'_c$  in equations (4) and (5), we find

$$\gamma'^2 - \alpha \frac{\gamma^2}{\epsilon + \gamma - a \xi \epsilon} \gamma' - (1 - b \xi) \alpha \epsilon \frac{\gamma^2}{\epsilon + \gamma - a \xi \epsilon} = 0 \tag{10}$$

and

$$RH' = 1 - \frac{1}{\gamma'} (1 - b \xi) \alpha \frac{\gamma^2}{\epsilon + \gamma - a \xi \epsilon}, \tag{11}$$

where  $b = e^{-\gamma' \Delta z}$ . If  $\Delta z = 0$ , then (10) is quadratic in  $\gamma'$  and can be solved analytically. If  $\Delta z \neq 0$ , then  $\gamma'$  also appears in  $b$ , which makes it necessary to solve (10) for  $\gamma'$  using a root solver. Aside from needing a numerical root solver for equation (10), everything else about this RCE model is analytical.

In general, the  $\delta D$  notation is related to the ratio of heavy mass fraction to light mass fraction by

$$\delta D = \frac{1}{R_{VSMOW}} \frac{18 q'}{19 q} - 1,$$

where  $R_{VSMOW}$  is the number concentration ratio for HDO versus  $H_2O$  in Vienna Standard Mean Ocean Water. Since

$$\frac{q'_c(z)}{q_c(z)} = \frac{q'_c(0)}{q_c(0)} e^{-(\gamma' - \gamma)z}$$

$$\frac{q'_e(z)}{q_e(z)} = \frac{RH' q'_c(0)}{RH q_c(0)} e^{-(\gamma' - \gamma)z},$$

the expressions for the cloud's  $\delta D_c$  and the environment's  $\delta D_e$  are

$$\delta D_c(z) = [1 + \delta D_c(0)] e^{-(\gamma' - \gamma)z} - 1 \quad (12)$$

$$\delta D_e(z) = \frac{RH'}{RH} [1 + \delta D_c(0)] e^{-(\gamma' - \gamma)z} - 1. \quad (13)$$

For  $\delta D_c(0)$ , we use  $-80\text{‰}$ , which is a typical value for tropical sub-cloud vapor (Galewsky et al., 2016).

### 3. The Weak Dependence of HDO on Convective Processes

Since the environment occupies the vast majority of the atmosphere, and since remote-sensing techniques retrieve  $\delta D$  in clear air, our focus is on  $\delta D_e$ . Our model for  $\delta D_e(z)$  is given by equation (13) in section 2, where the expressions for  $\gamma'$ ,  $RH$ , and  $RH'$  are given by equations (10), (7), and (11). Based on observations, we have set  $\gamma = 0.5 \text{ km}^{-1}$ ,  $\alpha = 1.17$ , and  $\delta D_c(0) = -80\text{‰}$ . That leaves three parameters ( $\epsilon$ ,  $\xi$ , and  $\Delta z$ ) upon which the solution for  $\delta D_e(z)$  depends. They relate to entrainment ( $\epsilon$ ), precipitation efficiency ( $1 - \xi$ ), and the falling or lofting of condensates ( $\Delta z$ ), three of the most uncertain and sought-after parameters in the study of deep convection (e.g., de Rooy et al., 2013; IPCC, 2013; Langhans et al., 2015; Lu et al., 2013, 2016; Romps, 2010, 2016a; Romps & Kuang, 2009; Tao et al., 2004).

Of course, we do have some a priori information about these parameters. From large-eddy simulations of tropical deep convection (Romps, 2010, 2014b), effective bulk-plume entrainment rates calculated from passive tracers tend to lie in the range of  $0.2\text{--}0.8 \text{ km}^{-1}$ . We select the middle of this range, i.e.,  $\epsilon = 0.5 \text{ km}^{-1}$ , as our best-guess value. Studies using cloud-resolving simulations of deep convection have variously reported precipitation efficiency to be 30–50% (Weisman & Klemp, 1982), 36–42% (Lipps & Hemler, 1986), 20–50% (Ferrier et al., 1996), 27% (Pauluis & Held, 2002), 32–45% (Tao et al., 2004), 21% (Romps, 2011), and 33–39% (Langhans et al., 2015). These results indicate that the precipitation efficiency  $1 - \xi$  lies in the range of 0.2–0.5. Therefore, the plausible range of  $\xi$  is 0.5 to 0.8, with a best-guess value of 0.65. For  $\Delta z$ , we can turn to the water-molecule-tracking large-eddy simulation of Langhans et al. (2015), which showed that the vast majority of liquid molecules that evaporate do so at a height below their height of condensation. Based on that analysis, we take a best-guess value of  $\Delta z$  to be 2 km. To be extremely conservative, however, we will set the plausible range of  $\Delta z$  to be any value greater than  $\log(\xi)/\gamma$ ; a  $\Delta z$  that is more negative than this lower bound will generate  $RH > 1$ . For  $\xi = 0.65$ ,  $\log(\xi)/\gamma$  equals  $-862$  meters. Therefore, plausible a priori ranges for the convective parameters are  $\epsilon \in [0.2, 0.8] \text{ km}^{-1}$ ,  $\xi \in [0.5, 0.8]$ , and  $\Delta z \in [\log(\xi)/\gamma, \infty]$ .

Let us take a look at some sample solutions to get a feel for how they depend on  $\epsilon$ ,  $\xi$ , and  $\Delta z$ . Figure 2a shows vertical profiles of  $\delta D_e(z)$  for the best-guess values of  $\xi = 0.65$  and  $\Delta z = 2 \text{ km}$ , and for four different values of  $\epsilon$ :  $0$ ,  $0.2 \text{ km}^{-1}$  (the lower bound on the plausible range),  $0.8 \text{ km}^{-1}$  (the upper bound on the plausible range), and  $\infty$ . The thickness of the curves increases with increasing  $\epsilon$ . Note that  $\delta D_e$  increases with increasing entrainment. This is because the detrainment rate equals the entrainment rate, and a higher detrainment rate dumps more relatively heavy cloud vapor (i.e.,  $q'_c > q'_e$ ) into the environment.

Figure 2b shows  $\delta D_e(z)$  for the best-guess values of  $\epsilon = 0.5 \text{ km}^{-1}$  and  $\Delta z = 2 \text{ km}$ , and for four different values of  $\xi$ :  $0$ ,  $0.5$  (the lower bound on the plausible range),  $0.8$  (the upper bound on the plausible range), and  $1$ .

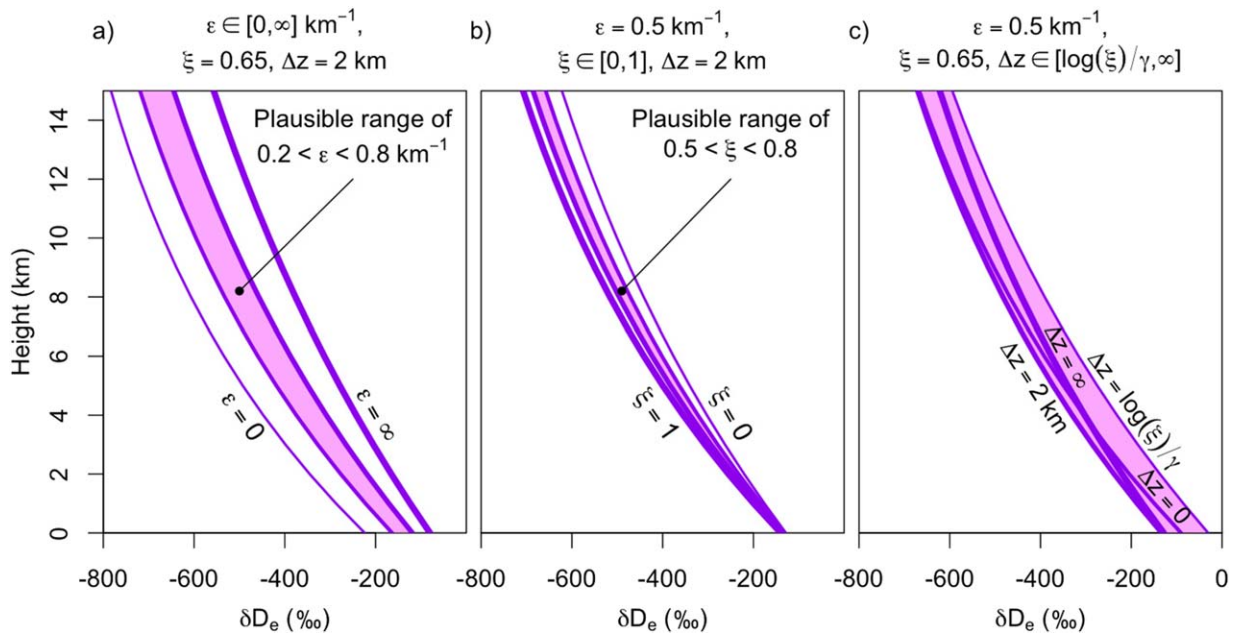


**Figure 2.**  $\delta D_e$  profiles calculated from the analytical model described by equations (7), (10), (11), and (13). Solid purple lines show the  $\delta D_e$  profiles for (a)  $\epsilon = 0, 0.2, 0.8, \text{ and } \infty \text{ km}^{-1}$  at the best-guess values of  $\xi = 0.65$  and  $\Delta z = 2 \text{ km}$ , (b)  $\xi = 0, 0.5, 0.8, \text{ and } 1$  at the best-guess values of  $\epsilon = 0.5 \text{ km}^{-1}$  and  $\Delta z = 2 \text{ km}$ , and (c)  $\Delta z = \log(\xi)/\gamma = -862 \text{ m}, 0, 2 \text{ km}, \text{ and } \infty$  at the best-guess values of  $\epsilon = 0.5 \text{ km}^{-1}$  and  $\xi = 0.65$ . The thickness of the purple line increases with increasing value of the parameter being varied. The regions shaded pink are the  $\delta D_e$  values corresponding to plausible parameter values.

The thickness of the curves increases with increasing  $\xi$ . We see that the environment becomes increasingly depleted as  $\xi$  is increased because, for  $\Delta z = 2 \text{ km}$ , the evaporating condensates are more depleted in HDO than the detraining water vapor (see Appendix B).

Finally, Figure 2c plots  $\delta D_e(z)$  for the best-guess values of  $\epsilon = 0.5 \text{ km}^{-1}$  and  $\xi = 0.65$ , and for four different values of  $\Delta z$ :  $\log(0.65)/\gamma = -862 \text{ m}$  (the value at which the environment becomes saturated), 0, 2 km (the best-guess value), and  $\infty$ . At a given height,  $\delta D_e$  is not monotonic in  $\Delta z$ , but the most depleted profile occurs for a  $\Delta z$  of approximately 2 km (see Appendix B), so the full range is filled out by these four profiles. Note that the  $\Delta z = \infty$  curve in Figure 2c is exactly the same curve as  $\xi = 0$  in Figure 2b; due to the Clausius-Clapeyron relation, there is zero condensation at infinite height, so there are no condensates to evaporate at finite  $z$  when  $\Delta z = \infty$ . The nonmonotonicity of  $\delta D_e$  with respect to  $\Delta z$  is explained in Appendix B.

The biggest takeaway from Figure 2 is just how small the variations in  $\delta D_e$  are over the plausible ranges of convective parameters. The plausible regions for  $\delta D_e$  are colored pink in each of the panels. The largest plausible variations in  $\delta D_e$  are in response to  $\epsilon$  and  $\Delta z$ , but  $\delta D_e$  changes by less than 75‰ as  $\epsilon$  is varied from its lower bound of  $0.2 \text{ km}^{-1}$  to its upper bound of  $0.8 \text{ km}^{-1}$ , and by less than 100‰ as  $\Delta z$  is changed from  $-862 \text{ m}$  to infinity. The response to changes in  $\xi$  is even smaller: less than 30‰ for the full range of plausible  $\xi$ . Given the measurement uncertainties and structural deficiencies of this and any other model of tropical convection, this does not bode well for the use of HDO measurements to constrain these convective parameters in a bulk-plume framework. In fact, as we will see in the next section, the profile of HDO adds little information about these processes that is not already present in the profile of  $\text{H}_2\text{O}$ .

#### 4. The Even Weaker Dependence Conditioned on RH

For HDO to be useful for studying convection, its mass fraction must tell us something that we cannot learn from the mass fraction of  $\text{H}_2\text{O}$  alone. To find out what additional information HDO provides, we must pick a value of RH and then look at all possible solutions with that RH (solutions to the analytical model have a constant RH profile and are thus characterized by a single RH value). For a given RH, there is a two-dimensional surface in the three-dimensional parameter space whose solutions all give that RH. For numerical models of the atmosphere, such as a cloud-resolving model or a single-column model with convective

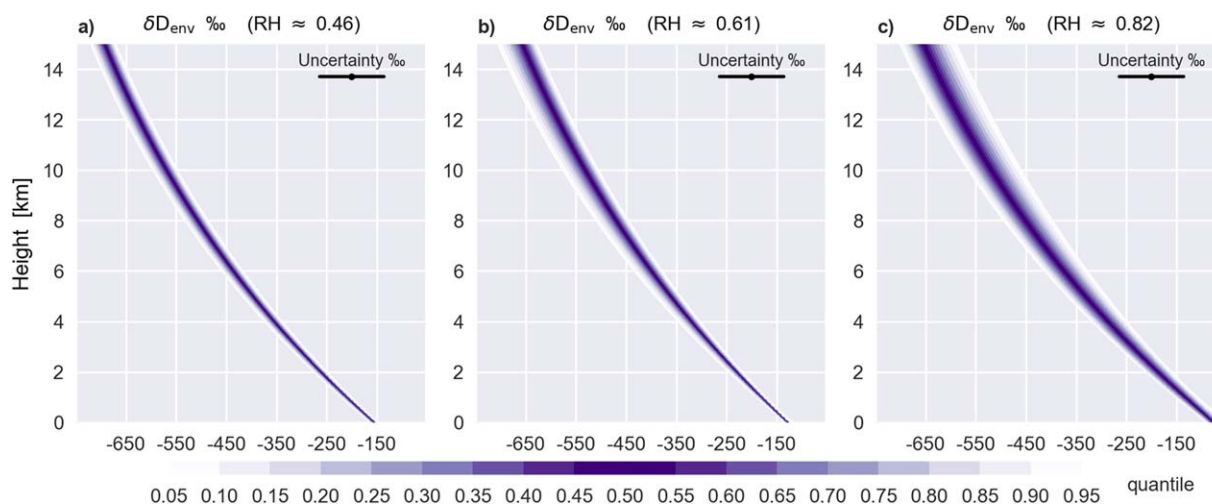


**Figure 3.** From physical solutions generated by sampling all possible combinations of evenly sampled  $\epsilon \in [0.2, 0.8] \text{ km}^{-1}$ ,  $\zeta \in [0.5, 0.8]$ , and  $\Delta z \in [\log(.5)/\gamma, 4 \text{ km}]$ , the shading shows the cumulative distribution function of  $\delta D_e$  for the subset solutions with an RH value at the (a) 10th percentile, (b) 50th percentile, and (c) 90th percentile of all physical RH values. The black bar in the upper right corner shows the estimate of the uncertainty in observing and modeling  $\delta D_e$ .

parameterization, it would be exceedingly difficult to map out that two-dimensional surface. For our analytical model, however, we can easily construct those two-dimensional surfaces by brute-force calculation.

We begin by generating approximately one million solutions to the analytical model given by equations (7), (10), (11), and (13). These solutions sample the parameter space on a regular grid, with 101 evenly spaced values of  $\epsilon$  from 0.2 to  $0.8 \text{ km}^{-1}$ , 101 evenly spaced values of  $\zeta$  from 0.5 to 0.8, and 101 evenly spaced values of  $\Delta z$  from  $\log(0.5)/\gamma$  to 4 km. We use  $\log(0.5)/\gamma$  as the lower bound for the range of  $\Delta z$  because, for  $\zeta \in [0.5, 0.8]$ , any value of  $\Delta z$  smaller than  $\log(0.5)/\gamma$  is guaranteed to give unphysical results (e.g.,  $\text{RH} > 1$ ). For the upper bound on  $\Delta z$ , we use 4 km, which is twice our best-guess value of 2 km. Sampling the parameter space in this way generates 1,030,301 solutions. Some of these solutions have  $e^{-\gamma\Delta z\zeta} > 1$ , which are unphysical solutions in the sense that they generate a relative humidity that is negative or greater than one. The existence of these unphysical solutions is not a failure of the model, but is, instead, the model's way of telling us that steady-state RCE is not possible for those parameter choices. For example, when  $\Delta z$  is too negative (i.e.,  $e^{-\gamma\Delta z\zeta}$  too big), there is no steady-state RCE solution: so much water is lofted from below that the subsidence "drying" cannot compete, and the atmosphere becomes progressively moister in a never-ending feedback loop. After we eliminate all solutions with  $e^{-\gamma\Delta z\zeta} > 1$ , we are left with 929,301 physical solutions.

Among the physical solutions, we identify the 10th, 50th, and 90th percentiles of RH. For each of those percentiles, we find the set of solutions whose RH lies within plus or minus one percentile of that value. This gives us three sets of 18,585 solutions each, with the solutions in each set having virtually identical RH. We can then look at the variations of  $\delta D_e$  within each set. The three panels in Figure 3 show the distributions of  $\delta D_e$  corresponding to the (a) 10th, (b) 50th, and (c) 90th percentile of RH, which correspond to relative humidities of 46%, 61%, and 82%, respectively. At each height, the shading corresponds to the quantile of the cumulative distribution function of the 18,585 profiles.

What does Figure 3 tell us? Imagine that we measured an RH of 61% in the tropical troposphere. This already tells us something about the possible values of  $\epsilon$ ,  $\zeta$ , and  $\Delta z$ : our observation of  $\text{H}_2\text{O}$  has restricted the possibilities to a two-dimensional surface in the three-dimensional parameter space. Now, we ask, can an observation of HDO restrict the possible parameter values to a one-dimensional curve on that surface? In principle, if we

assume that we can measure HDO exactly, and if we assume that the model is a perfect representation of reality, then the answer would be yes. But, in practice, there will always be measurement uncertainty in observations as well as parametric and structural uncertainty in models.

Table 1 quantifies those uncertainties. For the observational uncertainty, we use the uncertainty in the mean tropical  $\delta D_e$  value at

**Table 1**  
Sources of Uncertainty When Comparing Modeled  $\delta D$  to Observed  $\delta D$

Observational	Parametric	Structural	Total
$\pm 20\%$	$\pm 6\%$	$\pm 60\%$	$\pm 64\%$

5.5 km reported by the Tropospheric Emissions Spectrometer (TES) (Beer et al., 2001). Although individual TES  $\delta D_e$  profiles have an uncertainty of about  $\pm 23\%$  (i.e.,  $\pm 3\%$  uncertainty in the HDO/H<sub>2</sub>O ratio; Worden et al., 2012), the more important number for our purposes is the uncertainty in the bias of TES measurements, which, coincidentally, has been reported to be about  $\pm 20\%$  (Herman et al., 2014).

On the modeling side, there are two types of uncertainty: parametric and structural. With regards to the parametric uncertainty, we must, at the very least, account for the uncertainty in  $\alpha$  (the equilibrium fractionation factor during condensation) and  $\alpha_r$  (the fractionation factor during reevaporation; see Appendix A). Even if we prescribed  $\alpha$  as a function of temperature (which would be more accurate than using a constant value), there would still be an uncertainty of about 0.005 (estimated from empirical formulations of  $\alpha$  from different studies; see Figure 2 of Kakiuchi & Matsuo, 1979). So we take  $1.17 \pm 0.005$  as the uncertain range for  $\alpha$ . As for  $\alpha_r$ , it could be 1 if the evaporation is total, and slightly larger than  $\alpha$  if it is partial. We take [1, 1.175] as the uncertainty range for  $\alpha_r$ .

To translate these parametric uncertainties into uncertainties in  $\delta D_e$ , we discretize the uncertainty ranges of  $\alpha$  and  $\alpha_r$  into 101 values each and take the best-guess value for the other parameters ( $\gamma=0.5 \text{ km}^{-1}$ ,  $\epsilon=0.5 \text{ km}^{-1}$ ,  $\xi=0.65$ , and  $\Delta z=2 \text{ km}$ ). The resulting  $101 \times 101$  solutions all have the same RH (by construction), but different values of  $\delta D_e$ . The standard deviation of  $\delta D_e$  among these solutions is  $6\%$ . Since this only accounts for the uncertainty in two model parameters,  $6\%$  is a conservative estimate of the parametric uncertainty.

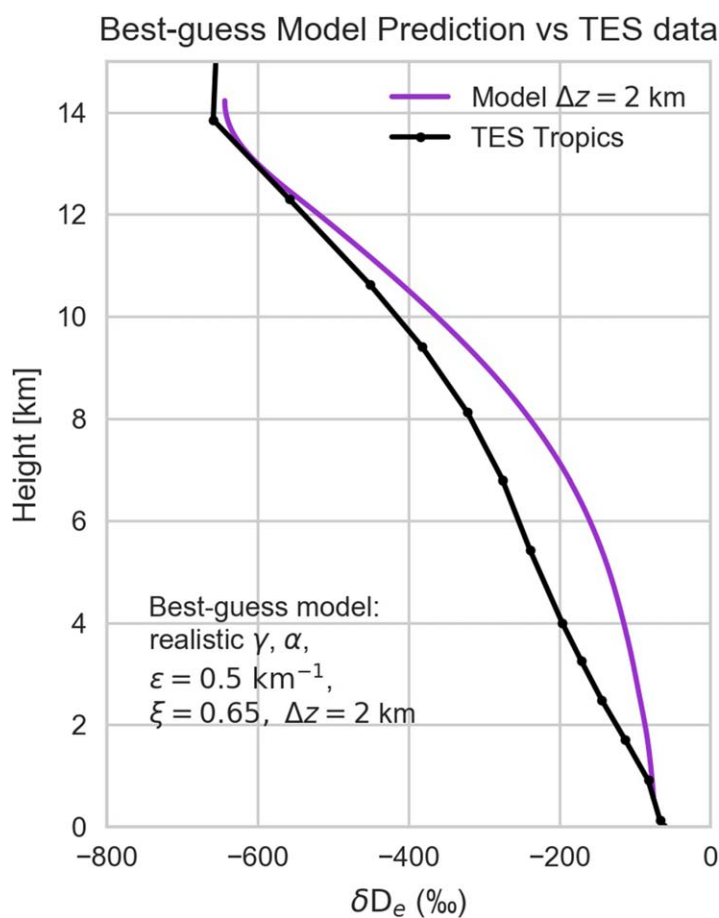


**Figure 4.** The profile of  $\delta D_e$  calculated from the numerical solution of the bulk-plume model (the purple curve) with observationally derived profiles of  $\alpha$  and  $q_c$  and with best-guess values of  $\epsilon=0.5 \text{ km}^{-1}$ ,  $\xi=0.65$ , and  $\Delta z=2 \text{ km}$ . Also shown (the black curve) is the profile of monthly mean  $\delta D$  retrieved from TES averaged over the tropics (20S–20N).

In any bulk-plume description of the tropical atmosphere, there will be many sources of structural uncertainty. One of the largest sources of structural uncertainty is the assumption in section 2 that the convective parameters (entrainment rate, precipitation efficiency, free-fall distance) are constant with height. These assumptions are unavoidable: making these parameters height-dependent would introduce even more unknown parameters that would render the task of learning anything from the isotopes all the more impossible.

To estimate the structural uncertainty, we can look at the mismatch in shape between the model's  $\delta D_e$  profile and observations. To minimize the mismatch, we can use realistic profiles of  $\alpha$  and  $q_c$ , although that forces us to integrate the model numerically. First, we prescribe the profiles of  $\alpha$  and  $q_c$  using the tropical-mean temperature and pressure profiles, with  $q_c$  set to the saturation water-vapor mass fraction. For the boundary conditions, we equate the properties of the cloud and environment at the tropopause and take the  $\delta D_e$  at the cloud base to be  $80\%$ , which is a typically observed value for  $\delta D$  of boundary-layer vapor in the tropics. Figure 4 illustrates the  $\delta D_e$  profile (the purple curve) calculated from the numerical model when taking the best-guess values of  $\epsilon=0.5 \text{ km}^{-1}$ ,  $\xi=0.65$ , and  $\Delta z=2 \text{ km}$ . The black curve is the monthly mean  $\delta D$  from TES retrievals averaged over the tropical domain ( $20^\circ\text{S}$ – $20^\circ\text{N}$ ). We estimate the structural uncertainty as the root-mean-square (RMS) of the difference at each TES retrieval level between the tropical-mean  $\delta D$  observed by TES and the  $\delta D_e$  calculated by the numerical model. The uncertainty calculated in this way is  $\pm 60\%$ .

As evidenced by the mismatch of profile shapes in Figure 4, there are refinements that could be added to the model that are capable of generating an isotopic effect of at least  $60\%$ . Those possible refinements include: treating convection as multiple plumes, each with its own mass flux and entrainment rate; modeling updraft speeds and their impact on condensate lofting; accounting for the 3D structure of clouds and precipitation fallout; and many more. Since it is unknown how to model or parameterize these refinements,  $\pm 60\%$  is a lower

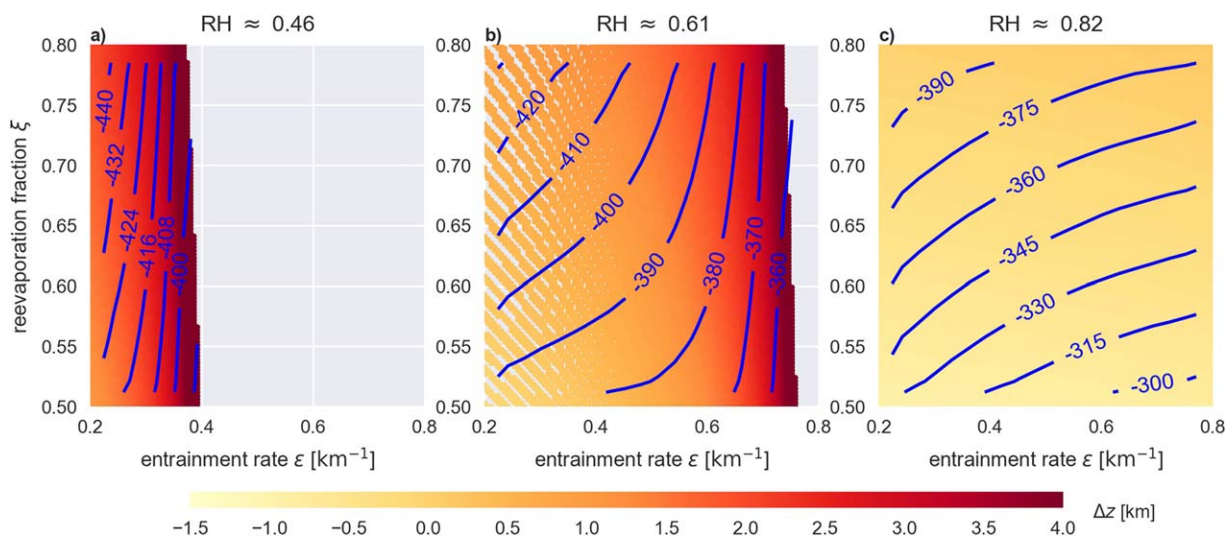


**Figure 5.** For each of the plots in Figure 3, the  $\epsilon$  (abscissa),  $\zeta$  (ordinate),  $\Delta z$  (color) of the 18,585 solutions with that RH. Overlaid on each of the plots are the contours of  $\delta D_e$  at 5.5 km.

bound on the uncertainty of the modeled isotope value in this or any more complicated parameterization of convection.

Therefore, combining the three uncertainties quantified above yields a conservative estimate of the true uncertainty. Summing the variances, we find that the uncertainty in  $\delta D_e$  is  $\pm \sqrt{6^2 + 60^2 + 20^2} \text{‰} \approx \pm 64 \text{‰}$ . We show this as the black bar at the top right in each panel of Figure 3.

In order for the tropical mean HDO to tell us something new about the bulk properties of convective processes, its modeled range at constant RH must be large compared to this uncertainty. Unfortunately, at fixed RH (i.e., within each panel of Figure 3), the variations in  $\delta D_e$  are smaller than or, at best, comparable to this uncertainty. In practice, therefore, the mean tropical HDO profile is unlikely to constrain convective processes in a bulk plume framework above and beyond what we can learn from relative humidity alone. If there is to be any success, however, Figure 3 hints that it will be found in moister conditions (Figure 3c exhibits a wider spread than Figure 3a) in the upper troposphere (in all panels of Figure 3, the spread is greatest near the tropopause). This is consistent with the notion that, in the moist TTL (above the free troposphere that we consider here), HDO is a promising candidate for telling us about moisture sources there (Bolot et al., 2017).

Figure 5a plots the two-dimensional surface in parameter space that corresponds to the 10th percentile of RH. This plot is constructed by adding a point for each of the 18,585 solutions at its corresponding  $(\epsilon, \zeta)$  coordinates and with a color corresponding to its  $\Delta z$ . Overlaid on this surface are contours of  $\delta D_e$  at 5.5 km, which is chosen because 5.5 km is a height where TES is most sensitive to  $\delta D_e$ . Note that, even if technical advances were to reduce the observational and model uncertainty to zero, knowing the precise  $\delta D_e$  contour would not uniquely identify the value of any of the three convective parameters. Figures 5b and 5c provide the same information for the 50th and 90th percentiles of RH.

### 5. Summary

We have derived an analytical model for profiles of  $\text{H}_2\text{O}$  and HDO in radiative-convective equilibrium, which is depicted in Figure 1. This model is defined by equations (7), (10), (11), and (13) in the section 2. Using these equations, we have generated solutions that explore the plausible range of three convective parameters: the entrainment rate ( $\epsilon$ ), the precipitation efficiency ( $1 - \zeta$ ), and the distance that condensates fall before evaporating ( $\Delta z$ ). These solutions, shown in Figure 2, show just how insensitive  $\delta D_e$  is to these convective parameters, which does not bode well for using measurements of HDO to constrain bulk convective processes. Matters get even worse when we conditionally sample solutions on an observed relative humidity. As shown in Figures 3 and 5, the variations of  $\delta D_e$  at a given RH are comparable to or smaller than the

uncertainty of observing (as estimated from the uncertainty in the TES  $\delta D_e$  bias) and modeling  $\delta D_e$  (as derived in section 4). Therefore, we conclude that the mean tropical free-tropospheric HDO profile is likely not useful for learning about the bulk properties of deep-convective processes.

## 6. Discussion

We have used a simplified model that focuses on the entrainment rate, precipitation efficiency, and the mean vertical displacement of condensates between condensation and evaporation. We have constant and equal entrainment and detrainment rates, which also yield a constant mass flux and a constant RH. Clearly, these simplifying choices have an impact on the detailed structure of the H<sub>2</sub>O and HDO profiles. The goal of this paper, however, is not to build the most detailed and accurate model of those profiles, but to explore the sensitivity of H<sub>2</sub>O and HDO to changes in the magnitude of the most basic and influential convective parameters. Adding additional complexity to the model would not increase the sensitivity of HDO to the magnitude of the entrainment rate and/or precipitation efficiency, but would increase the uncertainties due to the introduction of additional uncertain parameters. This would not increase the utility of HDO measurements; quite to the contrary, it would further obfuscate what the weak HDO signal is trying to tell us. In this sense, the analytical solutions presented above are a best case scenario for the utility of HDO measurements within the bulk-plume framework.

Indeed, we have explored numerical solutions that relax the simplifying assumption that certain key parameters are constant with height. For example, we used observational profiles of  $\alpha$  and  $q_c$  when calculating the structural uncertainty. Although not shown, we also tried an idealized fit of  $\epsilon$  as in Figure 6 of Romps (2014b). None of those sensitivity tests altered the conclusions; therefore, the paper has focused on the analytical solutions, which allow us to sample many thousands of solutions.

Some of the processes we did not model were the sources and sinks of HDO in the sub-cloud layer due to downdrafts and evaporation of precipitation. Note, however, that we have pegged the sub-cloud  $\delta D$  to the observed value, and that observed value incorporates those processes. The influence from the change of the source vapor in the boundary layer are beyond the scope of this study which focuses on the free troposphere. Another process not discussed in the text above was the fractionation during partial evaporation of condensates. Above 5 km, condensed water is mostly in the ice phase and the fractionation during partial evaporation is negligible (section 4.2 in Sherwood & Risi, 2012). Nevertheless, we have conducted sensitivity experiments by including a parameter  $\alpha_r$  to model fractionation during condensate evaporation; these results are given in Appendix A. Including this fractionation does not alter the conclusions.

Finally, we can ask how we might understand the model and the parameters  $\epsilon$ ,  $\xi$  and  $\Delta z$  in the context of the tropics. The bulk-plume model presented here can be thought of as representing the convecting tropics, such as the atmosphere over the warm pool, or as representing the entire tropics. In the latter case,  $\epsilon$ ,  $\xi$ , and  $\Delta z$  can be interpreted in the manner discussed by Romps (2014a) by thinking about entrained air as a mixture of subsaturated subtropical air and saturated air recently detrained by moist convection in the humid deep tropics. Although one could try to make that mapping quantitatively accurate, it is probably more useful to think of the simple model presented here as a way to illuminate the connections between basic convective processes and environmental HDO. The additional bells and whistles included in more complex models are unlikely to make the HDO signal easier to interpret in terms of fundamental convective processes. To the contrary, additional complexity simply introduces additional uncertainties that render the HDO signal even less prescriptive. And, as we have seen, even a very simple model has  $\delta D$  values that are stubbornly insensitive to the convective parameters of entrainment rate, precipitation efficiency, and vertical displacement between condensate formation and evaporation.

## Appendix A: Including Fractionation During Condensate Reevaporation

In the model used in the main text, it is assumed that a fraction  $\xi$  of hydrometeors are evaporated completely, which implies that there is no fractionation upon evaporation. Here, we will derive the equations for the case where a fraction  $\xi$  of each hydrometeor is evaporated, which does lead to additional fractionation. Although this increases the complexity of the model, we will see that this does not change our conclusions.

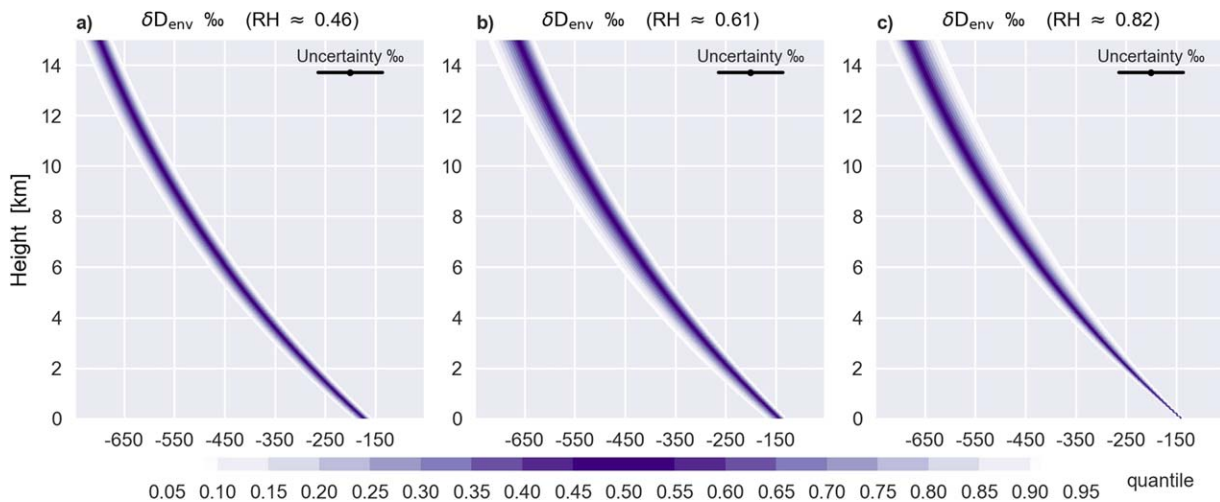


Figure A1. The same as Figure 3, but with fractionation during post-condensation evaporation, i.e.,  $\alpha_r > 1$ .

Consider a liquid drop in which  $N$  and  $N'$  denote the numbers of  $H_2O$  and HDO molecules, respectively. If  $dN$  of the drop evaporates, then the number of HDO molecules that evaporates is

$$dN' = dNR / \alpha_r,$$

where  $R = N' / N$  and  $\alpha_r = R_{\text{liquid}} / R_{\text{vapor}}$  is the (potentially nonequilibrium) fractionation factor during the evaporation of condensate. For a drop with initial abundances  $N_0$  and  $N'_0$ , we can integrate this to find that evaporating  $\xi$  of the drop, i.e.,  $N = (1 - \xi)N_0$ , leads to

$$N' = (1 - \xi)^{1/\alpha_r} N'_0.$$

Therefore, if a fraction  $\xi$  of the drop evaporates, the evaporated vapor has  $\xi$  of the drop's initial  $H_2O$  and  $1 - (1 - \xi)^{1/\alpha_r}$  of the drop's initial HDO. Therefore, equation (5) gets modified to

$$\frac{\partial}{\partial z} (-Mq'_e) = -\epsilon Mq'_e + \delta Mq'_c + \left[ 1 - (1 - \xi)^{1/\alpha_r} \right] \alpha \frac{q'_c(z + \Delta z)}{q_c(z + \Delta z)} C(z + \Delta z). \quad (A1)$$

Both  $\alpha$  and  $\alpha_r$  have a lower bound of 1. If  $\alpha_r$  takes a value of 1, then equation (A1) reverts to equation (5) with no fractionation during reevaporation. For raindrop evaporation in sub-saturated environment, the

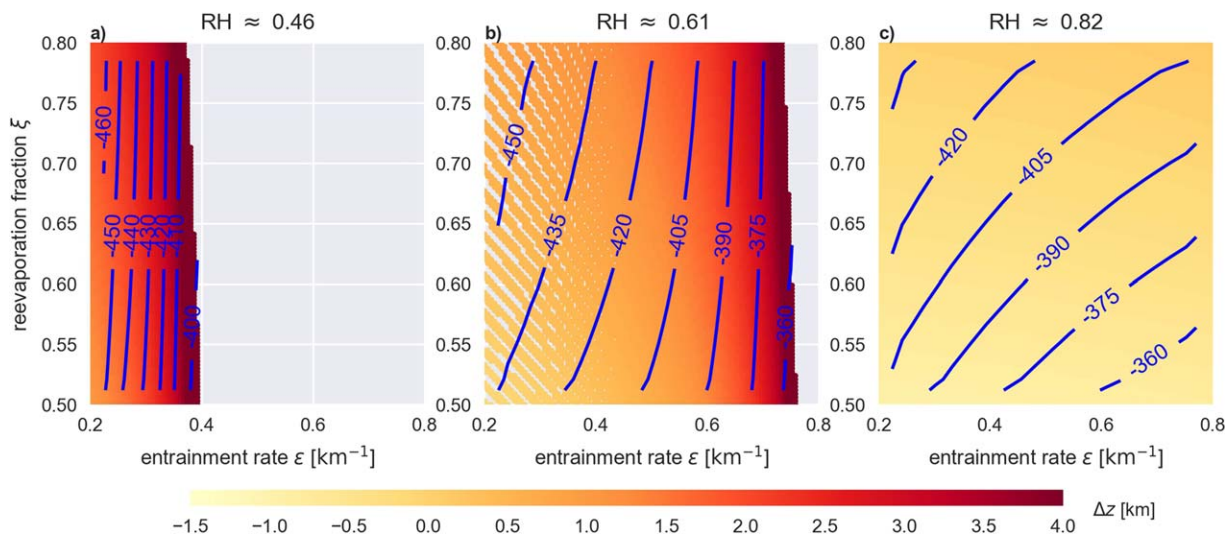


Figure A2. The same as Figure 5, but with fractionation during post-condensation evaporation, i.e.,  $\alpha_r > 1$ .

fractionation factor  $\alpha_r$  is slightly greater than the equilibrium fractionation factor  $\alpha$  (Bolot et al., 2013; Noone, 2012; Stewart, 1975). If we properly accounted for the additional uncertainty as to the value of  $\alpha_r$ , the connection between the HDO signal and the underlying physics would be further obscured: an observation of RH would only restrict us to a three-dimensional surface within a four-dimensional parameter space. We will, however, give HDO the best chance to provide useful information by assuming a single value for  $\alpha_r$ ; we will simply take  $\alpha_r = \alpha$ . With this choice, the distributions of  $\delta D_e$  profiles shown in Figure A1 are slightly wider, but the conclusion that their ranges are comparable to or smaller than the uncertainties is unaffected. Shown in Figure A2 is the underlying  $\epsilon$  (abscissa),  $\xi$  (ordinate),  $\Delta z$  (color) corresponding to Figure A1. Overlaid on each of the plots are the contours of  $\delta D_e$  at 5.5 km. Comparing Figures A1 and A2 to the original Figures 3 and 4, we see that the overall conclusion does not change after imposing  $\alpha_r > 1$ . The possible  $\delta D_e$  range for the full range of plausible parameter values in Figure A2 is everywhere less than 100‰, which is smaller than the uncertainty of observing and modeling  $\delta D_e$ .

### Appendix B: Nonmonotonic Change of $\delta D_e$ With $\Delta z$

In section 3, we saw that  $\delta D_e$  is nonmonotonic with respect to  $\Delta z$ . To understand this behavior, note that the  $\delta D$  values for the convective vapor at  $z$ , environmental vapor at  $z$ , convective condensates formed at  $z$ , and convective condensates formed at  $z + \Delta z$  (and evaporated at  $z$ ) are:

$$\delta D_c(z) = [1 + \delta D_c(0)]e^{-(\gamma' - \gamma)z} - 1$$

$$\delta D_e(z) = \frac{RH'}{RH} [1 + \delta D_c(0)]e^{-(\gamma' - \gamma)z} - 1$$

$$\delta D_{\text{conden}}(z) = \alpha [1 + \delta D_c(0)]e^{-(\gamma' - \gamma)z} - 1$$

$$\delta D_{\text{conden}}(z + \Delta z) = \alpha e^{-(\gamma' - \gamma)\Delta z} [1 + \delta D_c(0)]e^{-(\gamma' - \gamma)z} - 1.$$

At the same level  $z$ ,  $\delta D_{\text{conden}}(z) > \delta D_c(z) > \delta D_e(z)$ . What value of  $\Delta z$  would make  $\delta D_{\text{conden}}(z + \Delta z) < \delta D_c(z)$ ? We would need  $\alpha e^{-(\gamma' - \gamma)\Delta z} < 1$ , which is  $\Delta z > -\ln \frac{1}{\alpha} / (\gamma' - \gamma) \geq -\ln \frac{1}{\alpha} / (\alpha - 1)\gamma \approx 1.85$  km. When  $\Delta z > 1.85$  km, the condensate formed at  $z + \Delta z$  is more depleted than the cloud vapor at  $z$ . Therefore, for  $\Delta z > 1.85$  km, the condensate evaporated at  $z$  is more depleted than the cloud vapor at  $z$ .

In Figure 2c, to the right of curve  $\Delta z = 0$  (i.e., for increasingly negative  $\Delta z$ , implying condensates that loft before evaporating),  $\delta D_e(z)$  enriches monotonically with increasingly negative  $\Delta z$ . However, to the left of curve  $\Delta z = 0$  (i.e., for increasingly positive  $\Delta z$ , implying condensates that fall before evaporating),  $\delta D_e(z)$  does not change monotonically with  $\Delta z$ . Why is this? Note that in the formula for  $\delta D_e(z)$ , with fixed  $\delta D_c(0)$  and  $\gamma$ , the change of both the factor  $\frac{RH'}{RH}$  and the exponent  $\gamma'$  determine the change of  $\delta D_e(z)$ .  $\frac{RH'}{RH}$  decreases monotonically with  $\Delta z$  from our lower bound for  $\Delta z$  ( $\log(0.65)/0.5$ ) up to about 2 km; when  $\Delta z$  is greater than 2 km,  $\frac{RH'}{RH}$  is virtually constant. On the other hand,  $\gamma'$  is nonmonotonic; for the chosen  $\epsilon$  and  $\xi$  in Figure 2c,  $\gamma'$  peaks around  $\Delta z = 1$  km. The combined behavior of  $\frac{RH'}{RH}$  and  $\gamma'$  determines the nonmonotonicity of  $\delta D_e(z)$ .

We can understand the physical nature of this nonmonotonicity by considering a counterintuitive feature of Figure 2c. In the upper troposphere, the  $\delta D_e(z)$  profiles are more depleted when  $\Delta z = 0$  (which is when heavy condensates evaporate at the height where they formed) than when  $\Delta z = \infty$  (which corresponds to no condensate evaporation at all because no condensates form at  $z = \infty$ ). How can the evaporation of heavy condensates lead to a more depleted environment than a case with no evaporation of condensates? In the lower troposphere, the isotopic concentrations of the cloud vapor and condensates are determined by the  $\delta D$  of the sub-cloud layer, which is fixed here at  $-80$ ‰, so the evaporation of condensates does the expected thing: it enriches the environment vapor (in the formula for  $\delta D_e(z)$ , when  $z$  is small, the effect of the exponent is small). By the time a cloud parcel has reached the middle troposphere, however, it has been highly influenced by the environmental air it has entrained, and the entrainment has a depleting effect on the cloud vapor. With a moister environment due to the condensate evaporation, there is more depleted environmental vapor being entrained into the cloud. This depletes the cloud and – because the environmental air comes from detrained cloudy air – depletes the environment as well.

### Acknowledgments

S.Q.D. is grateful for the support of a State Scholarship Fund managed by the China Scholarship Council under grant 201406210235 for a one-year visiting student program to the University of California, Berkeley. S.Q.D. also acknowledges a PhD Student International Conference Fellowship from Tsinghua University, which supported return trips to Berkeley. This work was supported in part by the U.S. Department of Energy's Climate Model Development and Validation (CMDV), an Office of Science, Office of Biological and Environmental Research activity, under contract DE-AC02-05CH11231, in part by the National Natural Science Foundation of China, under grant number 41350110225, and by a Young Thousand Talents fellowship at Tsinghua University. TES data were acquired from the Aura Validation Data Center hosted by the NASA Goddard Space Flight Center (<http://avdc.gsfc.nasa.gov>). The authors thank N. Jeevanjee, W. Langhans, J. Seeley, J. Edman, P. Blossy, and L. Donner for helpful discussions. We thank two anonymous reviewers for their thoughtful discussion of the manuscript.

### References

- Beer, R., Glavich, T. A., & Rider, D. M. (2001). Tropospheric emission spectrometer for the Earth Observing System's Aura satellite. *Applied Optics*, *40*(15), 2356–2367.
- Berkelhammer, M., Risi, C., Kurita, N., & Noone, D. C. (2012). The moisture source sequence for the Madden-Julian Oscillation as derived from satellite retrievals of HDO and H<sub>2</sub>O. *Journal of Geophysical Research: Atmospheres*, *117*, D03106. <https://doi.org/10.1029/2011JD016803>
- Bolot, M., Legras, B., & Moyer, E. J. (2013). Modelling and interpreting the isotopic composition of water vapour in convective updrafts. *Atmospheric Chemistry and Physics*, *13*(16), 7903–7935. <https://doi.org/10.5194/acp-13-7903-2013>
- Bolot, M., Legras, B., Walker, K. A., Boone, C. D., Bernath, P., Read, W. G., & Moyer, E. J. (2017). Isotopic profiles imply strong convective influence on water near the tropical tropopause. *Proceedings of the National Academy of Sciences United States of America*. arXiv:1612.01900
- Bony, S., Risi, C., & Vimeux, F. (2008). Influence of convective processes on the isotopic composition ( $\delta^{18}\text{O}$  and  $\delta\text{D}$ ) of precipitation and water vapor in the tropics: 1. radiative-convective equilibrium and tropical ocean?global atmosphere?coupled ocean-atmosphere response experiment (toga-coare) simulations. *Journal of Geophysical Research: Atmospheres*, *113*, D19305. <https://doi.org/10.1029/2008JD009942>
- Brown, D., Worden, J., & Noone, D. (2008). Comparison of atmospheric hydrology over convective continental regions using water vapor isotope measurements from space. *Journal of Geophysical Research: Atmospheres*, *113*, D15124. <https://doi.org/10.1029/2007JD009676>
- de Rooy, W. C., Bechtold, P., Fröhlich, K., Hohenegger, C., Jonker, H., Mironov, D., et al. (2013). Entrainment and detrainment in cumulus convection: An overview. *Quarterly Journal of the Royal Meteorological Society*, *139*(670), 1–19. <https://doi.org/10.1002/qj.1959>
- Ferrier, B. S., Simpson, J., & Tao, W.-K. (1996). Factors responsible for precipitation efficiencies in midlatitude and tropical squall simulations. *Monthly Weather Review*, *124*(10), 2100–2125.
- Frappier, A. B., Sahagian, D., Carpenter, S. J., González, L. A., & Frappier, B. R. (2007). Stalagmite stable isotope record of recent tropical cyclone events. *Geology*, *35*(2), 111–114.
- Galewsky, J., Steen-Larsen, H. C., Field, R. D., Worden, J., Risi, C., & Schneider, M. (2016). Stable isotopes in atmospheric water vapor and applications to the hydrologic cycle. *Reviews of Geophysics*, *54*, 809–865. <https://doi.org/10.1002/2015RG000512>
- Herman, R. L., Cherry, J. E., Young, J., Welker, J. M., Noone, D., Kulawik, S. S., & Worden, J. (2014). Aircraft validation of Aura Tropospheric Emission Spectrometer retrievals of HDO/H<sub>2</sub>O. *Atmospheric Measurement Techniques*, *7*(9), 3127–3138.
- Higgins, P., & MacFadden, B. J. (2004). Amount effect" recorded in oxygen isotopes of Late Glacial horse (Equus) and bison (Bison) teeth from the Sonoran and Chihuahuan deserts, southwestern United States. *Palaeogeography, Palaeoclimatology, Palaeoecology*, *206*(3–4), 337–353.
- IPCC (2013). *Climate Change 2013: The Physical Science Basis. Contribution of Working Group I to the Fifth Assessment Report of the Intergovernmental Panel on Climate Change* (1535 pp.). Cambridge, UK: Cambridge University Press. <https://doi.org/10.1017/CBO9781107415324>
- Jouzel, J., Lorius, C., Petit, J. R., Genthon, C., Barkov, N. I., Kotlyakov, V. M., & Petrov, V. M. (1987). Vostok ice core: A continuous isotope temperature record over the last climatic cycle (160,000 years). *Nature*, *329*(6138), 403–408.
- Kakiuchi, M., & Matsuo, S. (1979). Direct measurements of d/h and 18o/16o fractionation factors between vapor and liquid water in the temperature range from 10 to 40. *Geochemical Journal*, *13*(6), 307–311.
- Kurita, N., Noone, D., Risi, C., Schmidt, G. A., Yamada, H., & Yoneyama, K. (2011). Intraseasonal isotopic variation associated with the Madden-Julian Oscillation. *Journal of Geophysical Research: Atmospheres*, *116*, D24101. <https://doi.org/10.1029/2010JD015209>
- Langhans, W., Yeo, K., & Roms, D. M. (2015). Lagrangian investigation of the precipitation efficiency of convective clouds. *Journal of the Atmospheric Sciences*, *72*(3), 1045–1062. <https://doi.org/10.1175/JAS-D-14-0159.1>
- Lee, J. E., Johnson, K., & Fung, I. (2009a). Precipitation over South America during the last glacial maximum: An analysis of the amount effect with a water isotope-enabled general circulation model. *Geophysical Research Letters*, *36*, L19701. <https://doi.org/10.1029/2009GL039265>
- Lee, J. E., Pierrehumbert, R., Swann, A., & Lintner, B. R. (2009b). Sensitivity of stable water isotopic values to convective parameterization schemes. *Geophysical Research Letters*, *36*, L23801. <https://doi.org/10.1029/2009GL040880>
- Lipps, F. B., & Hemler, R. S. (1986). Numerical simulation of deep tropical convection associated with large-scale convergence. *Journal of the Atmospheric Sciences*, *43*(17), 1796–1816.
- Lu, C., Liu, Y., Niu, S., Krueger, S., & Wagner, T. (2013). Exploring parameterization for turbulent entrainment-mixing processes in clouds. *Journal of Geophysical Research: Atmospheres*, *118*, 185–194. <https://doi.org/10.1029/2012JD018464>
- Lu, C., Liu, Y., Zhang, G. J., Wu, X., Endo, S., Cao, L., et al. (2016). Improving parameterization of entrainment rate for shallow convection with aircraft measurements and large-eddy simulation. *Journal of the Atmospheric Sciences*, *73*(2), 761–773. <https://doi.org/10.1175/JAS-D-15-0050.1>
- Moreira, M., Sternberg, L., Martinelli, L., Victoria, R., Barbosa, E., Bonates, L., & Nepstad, D. (1997). Contribution of transpiration to forest ambient vapour based on isotopic measurements. *Global Change Biology*, *3*(5), 439–450.
- Noone, D. (2012). Pairing measurements of the water vapor isotope ratio with humidity to deduce atmospheric moistening and dehydration in the tropical midtroposphere. *Journal of Climate*, *25*(13), 4476–4494.
- Nusbaumer, J., Wong, T. E., Bardeen, C., & Noone, D. (2017). Evaluating hydrological processes in the community atmosphere model version 5 (cam5) using stable isotope ratios of water. *Journal of Advances in Modeling Earth Systems*, *9*, 949–977. <https://doi.org/10.1002/2016MS000839>
- Pauluis, O., & Held, I. M. (2002). Entropy budget of an atmosphere in radiative-convective equilibrium. Part II: Latent heat transport and moist processes. *Journal of the Atmospheric Sciences*, *59*(2), 140–149.
- Petit, J. R., Jouzel, J., Raynaud, D., Barkov, N. I., Barnola, J.-M., Basile, I., et al. (1999). Climate and atmospheric history of the past 420,000 years from the Vostok ice core, Antarctica. *Nature*, *399*(6735), 429–436.
- Risi, C., Bony, S., & Vimeux, F. (2008). Influence of convective processes on the isotopic composition ( $\delta^{18}\text{O}$  and  $\delta\text{D}$ ) of precipitation and water vapor in the tropics: 2. Physical interpretation of the amount effect. *Journal of Geophysical Research: Atmospheres*, *113*, D19306. <https://doi.org/10.1029/2008JD009943>
- Risi, C., Bony, S., Vimeux, F., Frankenberg, C., Noone, D., & Worden, J. (2010). Understanding the Sahelian water budget through the isotopic composition of water vapor and precipitation. *Journal of Geophysical Research: Atmospheres*, *115*, D24110. <https://doi.org/10.1029/2010JD014690>
- Risi, C., Noone, D., Worden, J., Frankenberg, C., Stiller, G., Kiefer, M., et al. (2012a). Process-evaluation of tropospheric humidity simulated by general circulation models using water vapor isotopologues: 1. Comparison between models and observations. *Journal of Geophysical Research*, *117*, D05303. <https://doi.org/10.1029/2011JD016621>

- Risi, C., Noone, D., Worden, J., Frankenberg, C., Stiller, G., Kiefer, M., et al. (2012b). Process-evaluation of tropospheric humidity simulated by general circulation models using water vapor isotopic observations: 2. Using isotopic diagnostics to understand the mid and upper tropospheric moist bias in the tropics and subtropics. *Journal of Geophysical Research: Atmospheres*, *117*, D05304. <https://doi.org/10.1029/2011JD016623>
- Romps, D. M. (2010). A Direct Measure of Entrainment. *Journal of the Atmospheric Sciences*, *67*(6), 1908–1927. <https://doi.org/10.1175/2010JAS3371.1>
- Romps, D. M. (2011). Response of tropical precipitation to global warming. *Journal of the Atmospheric Sciences*, *68*(1), 123–138.
- Romps, D. M. (2014a). An analytical model for tropical relative humidity. *Journal of Climate*, *27*(19), 7432–7449. <https://doi.org/10.1175/JCLI-D-14-00255.1>
- Romps, D. M. (2014b). Rayleigh damping in the free troposphere. *Journal of the Atmospheric Sciences*, *71*(2), 553–565. <https://doi.org/10.1175/JAS-D-13-062.1>
- Romps, D. M. (2016a). The Stochastic Parcel Model: A deterministic parameterization of stochastically entraining convection. *Journal of Advances in Modeling Earth Systems*, *8*, 319–344. <https://doi.org/10.1002/2015MS000537>
- Romps, D. M. (2016b). Clausius-Clapeyron scaling of CAPE from analytical solutions to RCE. *Journal of the Atmospheric Sciences*, *73*(9), 3719–3737.
- Romps, D. M., & Kuang, Z. (2009). Nature versus nurture in shallow convection. *Journal of the Atmospheric Sciences*, *67*(5), 1655–1666. <https://doi.org/10.1175/2009JAS3307.1>
- Romps, D. M., & Öktem, R. (2015). Stereo photogrammetry reveals substantial drag on cloud thermals. *Geophysical Research Letters*, *42*, 5051–5057. <https://doi.org/10.1002/2015GL064009>
- Seeley, J. T., & Romps, D. M. (2016a). Why does tropical convective available potential energy (CAPE) increase with warming? *Geophysical Research Letters*, *42*, 10429–10437. <https://doi.org/10.1002/2015GL066199>
- Seeley, J. T., & Romps, D. M. (2016b). Tropical cloud buoyancy is the same in a world with or without ice. *Geophysical Research Letters*, *43*, 3572–3579. <https://doi.org/10.1002/2016GL068583>
- Sherwood, S. C., & Risi, C. (2012). The HDO/H<sub>2</sub>O relationship in tropospheric water vapor in an idealized “last-saturation” model. *Journal of Geophysical Research: Atmospheres*, *117*, D19205. <https://doi.org/10.1029/2012JD018068>
- Singh, M. S., & O’gorman, P. A. (2013). Influence of entrainment on the thermal stratification in simulations of radiative-convective equilibrium. *Geophysical Research Letters*, *40*, 4398–4403. <https://doi.org/10.1002/grl.50796>
- Steffensen, J. P., Andersen, K. K., Bigler, M., Clausen, H. B., Dahl-Jensen, D., Fischer, H., et al. (2008). High-resolution Greenland ice core data show abrupt climate change happens in few years. *Science*, *321*(5889), 680–684.
- Stewart, M. K. (1975). Stable isotope fractionation due to evaporation and isotopic exchange of falling waterdrops: Applications to atmospheric processes and evaporation of lakes. *Journal of Geophysical Research: Atmospheres*, *80*(9), 1133–1146.
- Tao, W. K., Johnson, D., Shie, C. L., & Simpson, J. (2004). The atmospheric energy budget and large-scale precipitation efficiency of convective systems during TOGA COARE, GATE, SCSMEX, and ARM: Cloud-resolving model simulations. *Journal of the Atmospheric Sciences*, *61*(20), 2405–2423.
- Tharammal, T., Bala, G., & Noone, D. (2017). Impact of deep convection on the isotopic amount effect in tropical precipitation. *Journal of Geophysical Research: Atmospheres*, *122*, 1505–1523. <https://doi.org/10.1002/2016JD025555>
- Thompson, L. G. O., Mosley-Thompson, E., Davis, M. E., Bolzan, J. F., Dai, J., Yao, T., et al. (1989). Holocene-late Pleistocene climatic ice core records from Qinghai-Tibetan Plateau. *Science*, *246*(4929), 474–477.
- Torri, G., Ma, D., & Kuang, Z. (2017). Stable water isotopes and large-scale vertical motions in the tropics. *Journal of Geophysical Research: Atmospheres*, *122*, 3703–3717. <https://doi.org/10.1002/2016JD026154>
- Weisman, M. L., & Klemp, J. B. (1982). The dependence of numerically simulated convective storms on vertical wind shear and buoyancy. *Monthly Weather Review*, *110*(6), 504–520.
- Williams, D. G., Cable, W., Hultine, K., Hoedjes, J. C. B., Yezpe, E. A., Simonneaux, V., et al. (2004). Evapotranspiration components determined by stable isotope, sap flow and eddy covariance techniques. *Agricultural and Forest Meteorology*, *125*(3), 241–258.
- Worden, J., Kulawik, S., Frankenberg, C., Payne, V., Bowman, K., Cady-Peirara, K., et al. (2012). Profiles of ch<sub>4</sub>, hdo, h<sub>2</sub>o, and n<sub>2</sub>o with improved lower tropospheric vertical resolution from aura tes radiances. *Atmospheric Measurement Techniques*, *5*(2), 397–411. <https://doi.org/10.5194/amt-5-397-2012>
- Worden, J., Noone, D., & Bowman, K. (2007). Importance of rain evaporation and continental convection in the tropical water cycle. *Nature*, *445*(7127), 528–532. <https://doi.org/10.1038/nature05508>
- Wright, J. S., Sobel, A. H., & Schmidt, G. A. (2009). Influence of condensate evaporation on water vapor and its stable isotopes in a GCM. *Geophysical Research Letters*, *36*, L12804. <https://doi.org/10.1029/2009GL038091>